Neuron
Report

Microstimulation Activates a Handful of Muscle Synergies

Simon A. Overduin,[1,*] Andrea d'Avella,[4] Jose M. Carmena,[1,2,3] and Emilio Bizzi[5]
[1]Department of Electrical Engineering and Computer Sciences
[2]Helen Wills Neuroscience Institute
[3]UCB-UCSF Joint Graduate Group in Bioengineering
University of California, Berkeley, Berkeley, CA 94720, USA
[4]Laboratory of Neuromotor Physiology, Santa Lucia Foundation, 00179 Rome, Italy
[5]Department of Brain and Cognitive Sciences and McGovern Institute for Brain Research, Massachusetts Institute of Technology, 43 Vassar Street, Cambridge, MA 02139, USA
*Correspondence: overduin@eecs.berkeley.edu
http://dx.doi.org/10.1016/j.neuron.2012.10.018

SUMMARY

Muscle synergies have been proposed as a mechanism to simplify movement control. Whether these coactivation patterns have any physiological reality within the nervous system remains unknown. Here we applied electrical microstimulation to motor cortical areas of rhesus macaques to evoke hand movements. Movements tended to converge toward particular postures, driven by synchronous bursts of muscle activity. Across stimulation sites, the muscle activations were reducible to linear sums of a few basic patterns—each corresponding to a muscle synergy evident in voluntary reach, grasp, and transport movements made by the animal. These synergies were represented nonuniformly over the cortical surface. We argue that the brain exploits these properties of synergies—postural equivalence, low dimensionality, and topographical representation—to simplify motor planning, even for complex hand movements.

INTRODUCTION

Complex movements are often described as the summation of simpler motor primitives. Typically, these modules have been defined in terms of overt movement kinematics, e.g., as patterns of force moving the limb to an equilibrium posture (Bizzi et al., 1991) or basic postural "synergies" composing hand movements (Mason et al., 2004; Santello et al., 1998). At a more fundamental level, motor primitives have also been defined as synergistic contractions of muscles (d'Avella et al., 2003; Drew et al., 2008; Kargo and Nitz, 2003; Brochier et al., 2004; Torres-Oviedo and Ting, 2007).

Electrical microstimulation studies have provided the most direct evidence that the nervous system encodes motor primitives. Whether applied intraspinally (Giszter et al., 1993; Aoyagi et al., 2004; Tresch and Bizzi, 1999; Zimmermann et al., 2011) or intracortically (Haiss and Schwarz, 2005; Ramanathan et al., 2006; Stepniewska et al., 2005; Graziano et al., 2002), suprathreshold microstimulation lasting several hundred milliseconds evokes complex multijoint forces that frequently drive the animal's body toward invariant postures.

These microstimulation studies have largely focused on overt movements rather than the underlying muscular control. Such kinematic studies have also concentrated on effectors with relatively few degrees of freedom. More complex convergent movements involving the macaque wrist and digits have been reported (Graziano et al., 2002, 2004a, 2005) but not yet quantified in a systematic manner. Moreover, while microstimulation is a valuable tool for causally probing neural function, it is unclear whether artificially elicited movements are a valid model of real behavior. In this study, we sought to address whether long-duration intracortical microstimulation (ICMS) would evoke naturalistic movements of the hand by recruiting muscles in a synergistic fashion.

RESULTS

We electrically microstimulated sites throughout the motor cortex of two rhesus macaques, "G1" and "G2" (Figure 1A). The animals were awake during ICMS and were either moving their arms or at rest in different postures. We considered 46 locations (G1: 33, G2: 13), mostly in primary motor cortex (MI: 32 sites), plus others in premotor cortex, both dorsal (PMd: 9) and ventral (PMv: 5). We stimulated each site with biphasic pulses (2 × 0.2 ms) at suprathreshold currents (8–100 μA) and an intermediate frequency (200 Hz) over multiple ($\geq$7), relatively long trains (150–500 ms). We recorded electromyograms (EMGs) from electrodes chronically implanted in forelimb muscles and (with G2) joint kinematics from a custom flex sensor glove.

We first investigated whether ICMS would move the hand toward specific final postures, as previously seen for limb movements. In all analyses, we focused on effects observed between 25 and 150 ms from the onset of stimulation, a duration in which we expected EMG responses to be relatively unaffected by voluntary reactions to ICMS (Nelson et al., 1990). The kinematic data from monkey G2 illustrate the pattern of movements noted for both animals. At each of G2's 13 stimulation sites, we applied ICMS trains with the hand at rest at different starting postures.

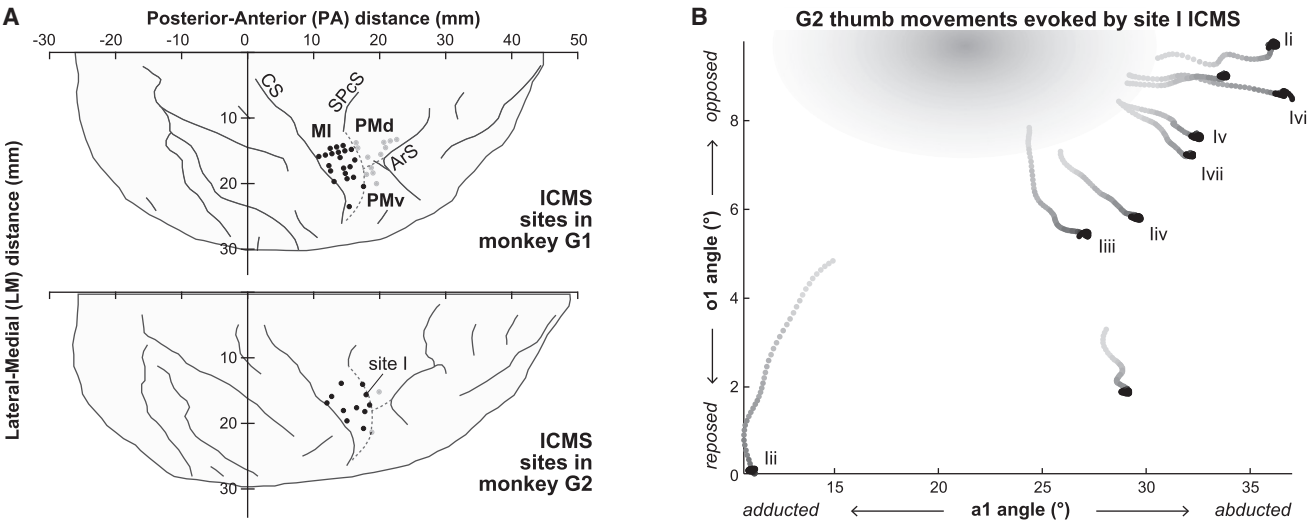

Figure 1. ICMS-Evoked Hand Movements Converged toward a Posture Unique to Each Site

(A) ICMS sites in monkey G1 (top) and G2 (bottom) are depicted as dots (MI: black, PMd/v: gray). Solid lines show sulci (CS, central; SPcS, superior precentral; ArS, arcuate); dashed lines depict estimated borders between cortical areas MI, PMd, and PMv. Label I indicates one sample site in G2's MI. (B) ICMS at G2's site I drove the hand toward a convergent posture. The hand was placed at a different initial posture prior to each ICMS train (black dots). The successively lighter gray dots extending from each initial posture show the hand's movement over the first 150 ms of ICMS. The shaded ellipse represents the mean ± SD of the intersections of straight lines connecting the beginning and end of each ICMS trace.

Pre-ICMS joint positions varied over 19° ± 11° (mean ± SD, range 4°–50° over sites and trains). The trains elicited 20° ± 18° (range 4°–55°) of (2-norm) movement over the joints. Regardless of the initial hand posture, ICMS at most sites evoked convergent motions of one or more joints. At the site shown in Figure 1B, for instance, ICMS drove the thumb toward a posture defined by relative opposition (joint o1) and intermediate abduction (a1). The dispersion of hand postures around their mean was reduced over the 150 ms of ICMS, by a significant degree in both joint dimensions shown ($p < 0.05$). Over the 13 stimulation sites in G2, such convergence was observed among 3.2 ± 2.9 of the 8–9 joints measured per site (range 0–9).

We next examined the patterns of muscle activity underlying such movements. We considered only the first seven ICMS trials (the minimal number available) per stimulation site. As illustrated in Figure 2A, the evoked EMG varied little from one stimulation train to the next. We defined ICMS-evoked EMG vectors by integrating the data of each of the electrodes (G1: 15, G2: 19) between 25 and 150 ms into each ICMS train (i.e., the vertical black-to-gray columns of EMG in Figure 2A). Comparing all pairs of vectors at a given site yielded pairwise dot products that averaged 0.95 ± 0.04 across sites for G1 (range 0.86–0.99) and 0.97 ± 0.02 for G2 (0.94–0.99). While the vectors were stable over stimulation trains, they nevertheless differed between sites. Average EMG vectors for each of G2's ICMS locations are shown in Figure 2B. Each site yielded a unique balance of activation across a number of muscles spanning multiple joints.

The foregoing analysis suggested that each ICMS site was defined by both a unique convergent posture and a unique balance of activity across muscles. But did these microstimulation-driven EMGs bear any resemblance to muscle activity observed in natural behavior? We inspected muscle data collected from the same animals while they performed a behavioral task prior to each of the ICMS sessions. The task required reach, grasp, and transport of 25 cylinders, cubes, and spheres between two wells (Figure 3A). We computed the average EMG activity across 40 trials performed with each of the 50 object shape, size, and position combinations. This EMG activity averaged 30μV ± 23μV for G1 (range 5μV–50μV over muscles) and 44μV ± 46μV for G2 (4μV–153μV), exceeding but overlapping with the activity evoked by ICMS: 10μV ± 10μV for G1 (2μV–28μV) and 16μV± 21μV for G2 (1μV–50μV). We found that the EMG data could be compactly represented by combinations of a small number of synchronous synergies, each a vector capturing a pattern of invariant coactivation across muscles. We used nonnegative matrix factorization (NNMF) to extract as many of these "grasp-related" synergies as needed to capture at least 95% of the variance in the EMG data (10 for G1, 8 for G2; Figure 3B).

To directly compare the grasp-related and ICMS-evoked EMG patterns, we likewise reduced the latter data into a smaller set of synergistic bases using NNMF. As we had observed for the grasp-related muscle data, the ICMS-evoked EMG vectors could be decomposed into a small number of "ICMS-derived" synergies (7 for G1, 6 for G2) with ≥95% of the EMG variability accounted for (Figure 3C). But more striking than the comparable dimensionality of the grasp-related and ICMS-evoked EMG data was the correspondence of the extracted dimensions themselves. We used a greedy search procedure to iteratively find the best-matching pairs of grasp-related and ICMS-derived synergies (Figure 3D). For G1 and G2, 6/7 and 6/6 of the ICMS-derived synergies could be matched with a corresponding grasp-related synergy. (Monkey G1's seventh

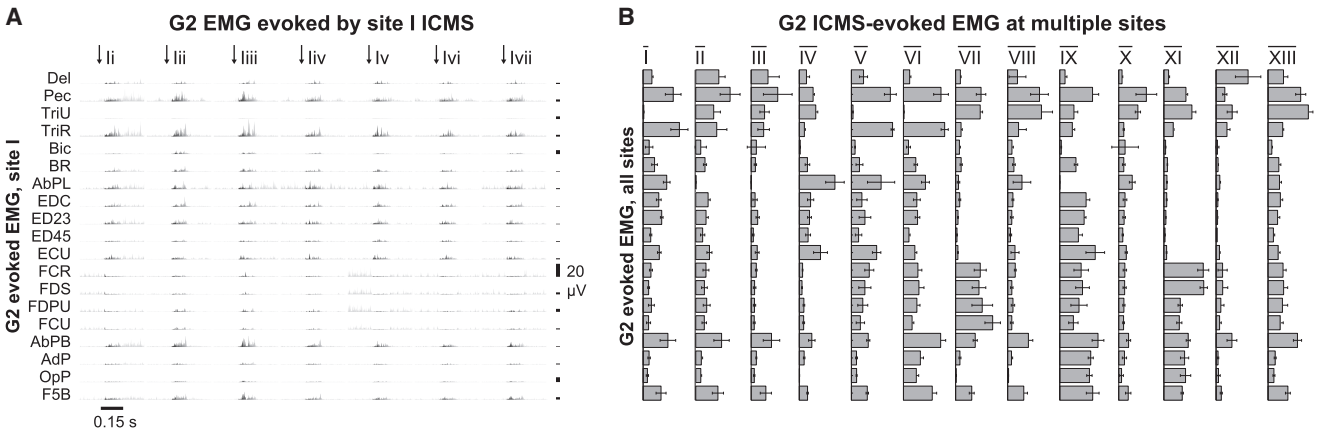

Figure 2. ICMS-Evoked Muscle Patterns Were Invariant and Unique to Each Site

(A) Each ICMS train at a cortical site evoked a muscle pattern that varied little with the hand's starting posture. Each plot shows EMG activity in the muscle abbreviated on the left, as measured from 150 ms before to 150 ms after each of seven ICMS trains delivered (at the times indicated by the black arrows) to a sample stimulation site (monkey G2's site I from Figure 1). The black-to-gray shading highlights EMG activity from 25 to 150 ms after onset (coincident with the movements in Figure 1B), which was integrated to define this site's ICMS-evoked EMG vectors. The 20μV scale bars on the right indicate the voltage scale for individual channels. (B) ICMS at different locations evoked different patterns of integrated muscle activity, shown here for all 13 stimulation sites in G2. Each vector shows the mean ± SD of the EMG activity evoked over seven ICMS trains delivered at the site.

ICMS-derived synergy is shown with the remaining, insignificantly matched grasp-related synergy.) The pairings yielded dot products averaging 0.86 ± 0.05 (range 0.81–0.93) for G1 and 0.83 ± 0.05 (0.75–0.92) for G2 and were each significant ($p < 0.05$) with reference to bootstrap populations of EMG-shuffled synergies.

Finally, we examined whether these ICMS-derived synergies were represented in any organized fashion on the cortical surface. The topographical data in Figure 4 suggest that this may have been the case. The sites evoking a synergy tended to cluster nonuniformly, at least in MI where most were located. For each site and ICMS-derived synergy, we calculated the mean synergy scaling coefficient necessary to reconstruct the evoked EMG activity over seven ICMS trains. We deemed to be significantly nonuniform any topographical map containing a mean coefficient exceeding a 95th percentile chance threshold, based on a population of coefficients drawn randomly from a uniform distribution. For monkey G1 and G2, 6/7 and 6/6 of the ICMS-derived synergies were associated with a significantly nonuniform representation peaking in MI.

DISCUSSION

There are at least three aspects of these results that are surprising. First, we found systematic evidence that ICMS can drive the hand, including digits, toward particular postures (Figure 1B). ICMS-evoked hand postures including precision and power grips have previously been observed (Graziano et al., 2002, 2004a, 2005; Ramanathan et al., 2006) but not studied in detail. That ICMS could evoke convergent movements of the hand, as had earlier been reported for more proximal limb and axial movements, is nonobvious. In primates, much of motor cortex is specialized for controlling the forelimb, especially the hand (Lemon, 1993). This control is facilitated by direct corticomotoneuronal projections to the spinal cord (Fetz and Cheney, 1978) that may enable muscular coordination unconstrained by evolutionarily primitive synergies encoded downstream of cortex (Rathelot and Strick, 2009). The stimulation sites in our study were primarily located in superficial motor cortex, rather than the rostral bank of the central sulcus from which most corticomotoneuronal projections originate. The convergent hand movements we observed may thus reflect motor primitives unobscured by these pathways.

Second, the muscle activations underlying these convergent movements had much in common with those seen in natural behaviors (Figure 3), however "unnatural" the neural activity induced by ICMS (Strick, 2002). It could have been the case that convergent postures are a trivial biomechanical result of imposing artificial patterns of tonic muscle contraction. Instead, we found that the evoked EMG patterns resembled muscle coactivations seen in temporally complex behaviors like reach and grasp. Our findings extend existing behavioral evidence that microstimulation-evoked force-field primitives (Giszter et al., 1993), bell-shaped speed profiles (Graziano et al., 2005), postural synergies (Gentner and Classen, 2006), and invariant endpoints (Graziano et al., 2004a) all tend to coincide with movements and postures found in spontaneous behavior. Consistent with the role of evoked motor primitives in simplifying motor control, other investigators have noted that when microstimulation is applied at multiple points in the spinal cord (Tresch and Bizzi, 1999) or motor cortex (Ethier et al., 2006), the final posture, convergent forces, and EMG activity all tend to sum linearly across sites. Precisely how long-train ICMS-evoked EMG yields invariant final postures remains to be explored, as does the extent to which this EMG changes with initial posture—variously found to be little (Loeb et al., 1993; Griffin et al., 2011), modest (Mussa-Ivaldi et al., 1990), or considerable (Graziano et al., 2004b).

Third, we were surprised to find a nonuniform representation of most ICMS-derived synergies (Figure 4), given long-standing

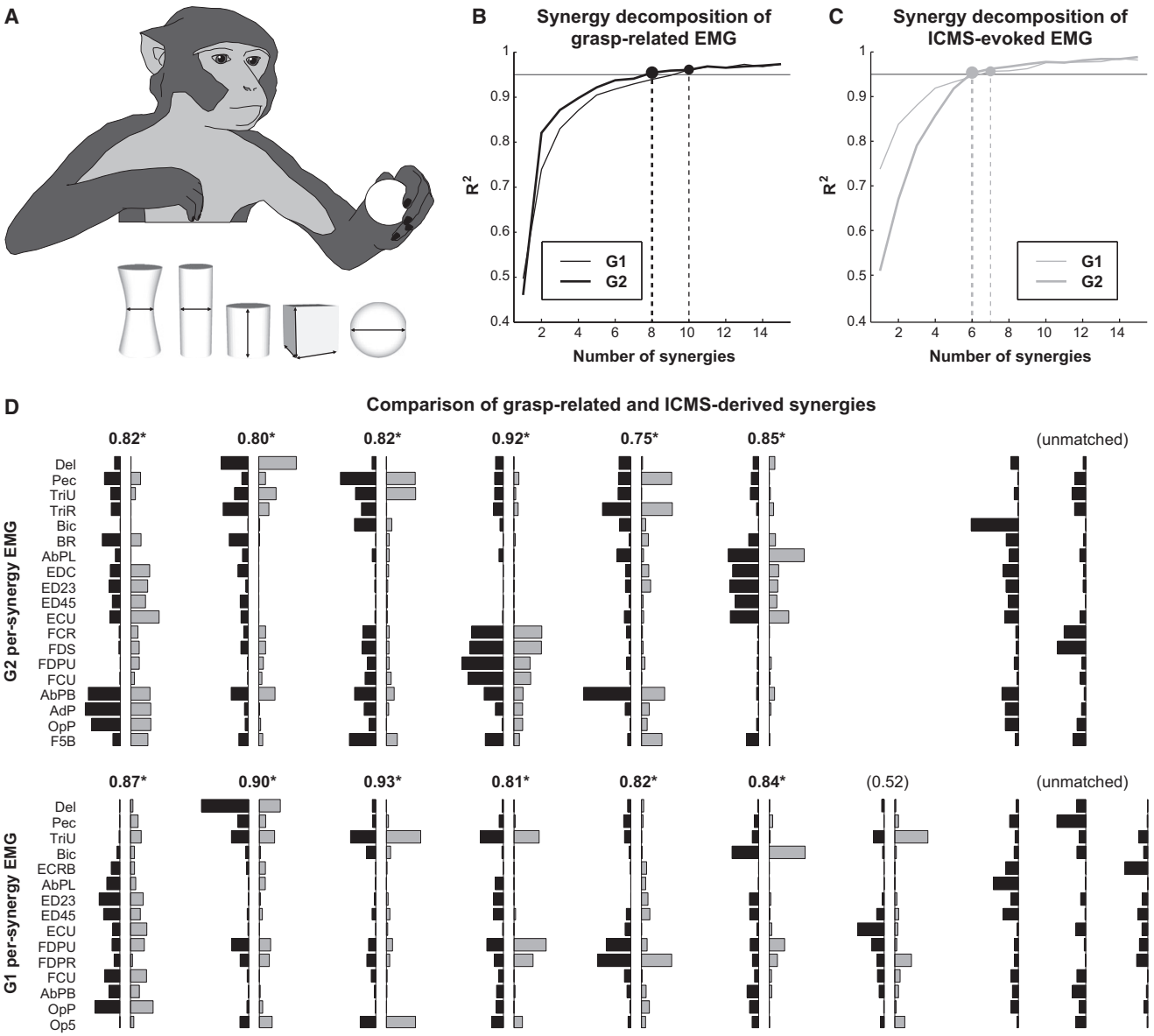

Figure 3. ICMS-Evoked Muscle Patterns Could Be Decomposed into a Small Set of Synergies Mirroring Those in Natural Behavior

(A) Monkey G1 is shown grasping one object, along with the shapes presented to both animals: cylinders of variable concavity, width, and height and cubes and spheres of variable size. (B) Ten (G1) or eight (G2) grasp-related synergies extracted from each monkey's EMG activity during the task could reconstruct these data with over 95% of EMG variance explained. (C) A slightly smaller number of synergies (seven or six) could explain over 95% of the variability in each monkey's population of ICMS-evoked EMG vectors. (D) The grasp-related synergies (in black, reflected along the ordinate) are shown paired together with the best-matching ICMS-derived synergies (gray). Numbers above the bar plots give their dot product; asterisks indicate significant correlations. Synergies have been ordered left to right by decreasing between-subject similarity of the ICMS-derived synergies (as measured by dot products, data not shown, of 0.86, 0.86, 0.74, 0.52, 0.48, and 0.08).

disagreements about whether motor cortex is organized topographically or is even divisible into functionally distinct areas—and about what motor cortex represents in the first place (Schieber, 2001; Graziano and Aflalo, 2007). Moreover, we had little reason to expect that motor cortex would encode muscle synergies, despite observing that ICMS-evoked EMG patterns could be resolved into such primitives (Figure 3). Instead, synergies may be encoded, if anywhere, downstream of motor cortex, in the brainstem (Roh et al., 2011) or spinal cord (Tresch et al., 1999; Saltiel et al., 2001; Hart and Giszter, 2010). The spinal cord may organize even distal forelimb synergies, as it contains premotor interneurons facilitating multiple muscles including ones intrinsic to the hand (Takei and Seki, 2010). Nor is cortex needed for convergent-movement primitives, as these can be evoked by long-train microstimulation in—or even downstream of—the spinal cord (Giszter et al., 1993; Aoyagi et al., 2004).

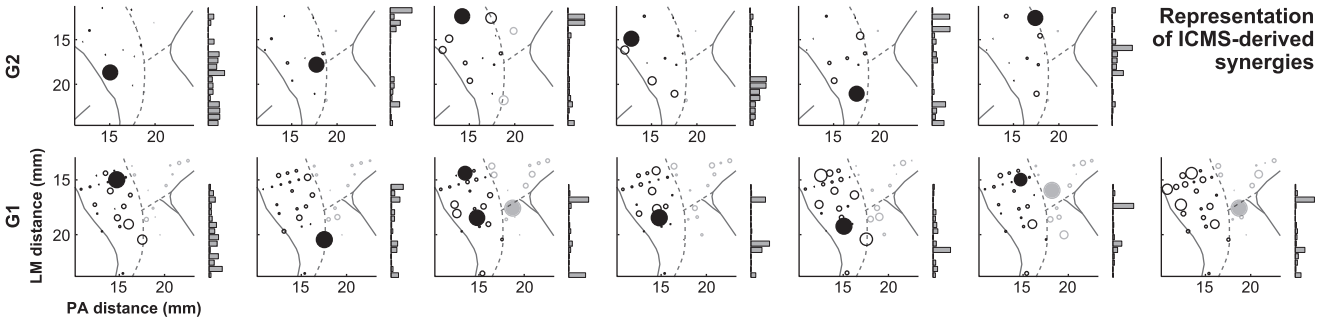

Figure 4. The Synergies Underlying the ICMS-Evoked Muscle Activity Were Represented Nonuniformly over the Cortical Surface

In each panel, the gray bar plot on the right reprints one of the seven (monkey G1) or six (G2) synergies that explained ≥95% of the variance among the ICMS-evoked EMG vectors. In the topographical plots to the left of each bar plot, black (MI) and gray (PMd/v) circles represent stimulation sites (as in Figure 1A). The size of each circle indicates the degree to which the site's evoked EMG activity was composed of the synergy shown on the right. (Specifically, the area of each circle is proportional to the scaling coefficient used in reconstructing the ICMS-evoked EMG vectors at that site and with that synergy, averaged over ICMS trains and normalized by the largest such circle within the plot.) Filled circles indicate locations with associated coefficients significantly larger than would be consistent with a uniform representation of the synergies.

The activations we evoked may thus be the result of filtering projections from motor cortex through neuromuscular webs that bind muscles together. Rather than encoding synergies directly, the primate's cortical specialization for forelimb behaviors may reflect its capacity to combine lower-level synergies into adaptive motor sequences (Overduin et al., 2008).

EXPERIMENTAL PROCEDURES

Subjects

Data were collected from two rhesus macaques (*Macaca mulatta*): "G1" (5.9 kg, 8 years old) and "G2" (6.5 kg, 4 years old, male). All procedures were approved by the MIT Committee on Animal Care.

Surgery

Muscle implantation surgeries are described in detail elsewhere (Overduin et al., 2008). Cranial surgeries were performed under sterile conditions and general anesthesia (0.05 mg/kg atropine and 10 mg/kg ketamine injected intramuscularly, followed in G1 by 5 mg/kg sodium pentobarbital intravenously and in G2 by inhalation of 1%–2% isoflurane with 2 l O_2). Craniotomies (20–28 mm wide) and stainless steel wells were centered over motor cortex in the right hemisphere. The animals were given analgesics and systemic antibiotics after surgeries.

Cortical Mapping

Areas MI, PMd, and PMv were identified by MRI data and by sensorimotor mapping using both peripheral sensory and intracortical electrical stimulation (Figure 1A). The sensorimotor mapping took place both during initial mapping studies and during the subsequent experimental sessions. This mapping used tungsten microelectrodes, each having a 50 μm shaft diameter tapered to a 3-μm-wide tip and 0.3–3 MΩ impedance (FHC). In each session, up to ten such electrodes were introduced perpendicularly into the brain using manual microdrives (30 μm depth resolution, spaced ≥1 mm apart). Once the electrodes had been lowered into cortex, the somatosensory response fields of cortical units near the electrodes were estimated by alternatively moving the monkeys' limbs and passively stimulating the skin. At the end of the sessions, the same electrodes were used to apply relatively short-train, high-frequency ICMS for mapping purposes. This form of ICMS (and not the longer-train, lower-frequency ICMS whose effects are the focus of this study) consisted of 2 × 0.2 ms cathodal-leading biphasic pulses of 1–150 μA current, presented in 50 ms trains at a 330 Hz pulse frequency. The pulses were created by staggering two pulse trains (Grass Technologies) and inverting the polarity of one train (BAK Electronics).

Grasping Task

Monkeys G1 and G2 participated in 19 and 9 experimental sessions spanning 50 and 15 days, respectively. During each session, subjects performed a learned behavior in which they had to press a start button and then reach for, grasp, and transport one of 25 objects of various sizes and shapes (Figure 3A) between two wells on either side of their midline. A separate analysis of a portion of these grasping-related data has previously been reported (Overduin et al., 2008). The data used here comprise 2,000 successful trials from each animal, including 40 trials in each of the 50 = 5 × 5 × 2 (object shape × size × position) conditions.

Microstimulation Delivery

At the end of the experimental sessions, the cortex was stimulated using relatively long trains of intermediate-frequency pulses, as compared to the ICMS used for sensorimotor mapping and described above. This ICMS consisted of 2 × 0.2 ms cathodal-leading biphasic pulses presented in 150 to 500 ms trains at a 200 Hz pulse frequency. Regardless of the train length, the analysis here focuses on data collected between 25 and 150 ms into each ICMS train or "trial." Currents were fixed at 100 μA, except for the first 9 of G1's 33 sites, for which they were set between 8–80 μA. Currents were at or above the 28 ± 24 μA (3–100 μA) thresholds at which movement could be reliably evoked by short-train, high-frequency ICMS (used for cortical mapping) when applied in rising increments of 10:10:100 μA (G1) or 25:25:100 μA (G2), for all but 3 (G1) and 6 (G2) sites at which thresholds were unspecified (i.e., >100 μA). For G1, trains were delivered periodically (once every 1 s) while the animal was either at rest or engaged in a food retrieval task (wherein dried fruit morsels were placed in the task wells instead of objects and were transported by the animal to its mouth rather than the opposing well). For G2, trains were delivered every few seconds at times chosen by the experimenter while the monkey's forelimb was at rest after being positioned and released at different postures.

Microstimulation Trials

For both animals, analysis was restricted to locations at which ≤100 μA long-train ICMS could reliably evoke movement on a majority of trials. As G1's ICMS was sometimes delivered while it was moving, those trains preceded by relatively large-amplitude movements were excluded to better equate its remaining trials with those of G2. For each EMG channel and stimulation site, muscle activity in the [–250:0] ms period just prior to ICMS was compared to a threshold (the root-mean-square EMG level over a [–250:+750] ms window around each ICMS train onset, concatenated over trains). These threshold values averaged 22μV ± 18μV (range 8μV–48μV over channels). G1's remaining 23 ± 15 ICMS trials per site (range 7–63), as well as G2's 13 ± 3 trials (9–17), were deemed to have had insignificant forelimb movement immediately prior to ICMS. Subsequent analysis of EMG data was limited to those locations

at which at least seven ICMS trials were available and to the first seven trials at each such site. These sites included 33 from G1 (MI: 21, PMd: 8, PMv: 4) and 13 from G2 (MI: 11, PMd: 1, PMv: 1).

Kinematic Data

Joint movements were recorded from monkey G2 using a custom flex sensor glove (and preprocessed as in Overduin et al., 2010). Nine sensors embedded in the glove sampled extension/flexion and ulnar/radial deviation (i.e., adduction/abduction) of the wrist (sensors eW and dW); carpometacarpal opposition/reposition of digit 5 (o5); flexion/extension at the metacarpophalangeal joints of digits 5, 3, 2, and 1 (f5, f3, f2, and f1); and trapeziometacarpal abduction/adduction and opposition/reposition of digit 1 (a1 and o1). (The f3 channel was not available during stimulation at 3 of the 13 sites.)

EMG Channels

EMG data were recorded through 15 (G1) or 19 (G2) electrodes chronically implanted in left forelimb muscles. Proximal muscles acting on the shoulder and elbow included Del (deltoideus), Pec (pectoralis major), TriU and TriR (triceps brachii, ulnar and radial short heads), Bic (biceps brachii longus), and BR (brachioradialis). Wrist and extrinsic hand extensors included AbPL (abductor pollicis longus) and extensors ECRB (carpi radialis brevis), EDC (digitorum communis), ED23 (digiti secundi and tertii proprius), ED45 (digiti quarti and quinti proprius), and ECU (carpi ulnaris). Wrist and extrinsic hand flexors included FCR (carpi radialis), FDS (digitorum superficialis), FDPU and FDPR (digitorum profundus, ulnar and radial), and FCU (carpi ulnaris). Intrinsic hand muscles included AbPB (abductor pollicis brevis), AdP (adductor pollicis), OpP (opponens pollicis), F5B (flexor digiti quinti brevis manus), and Op5 (opponens digiti quinti manus).

EMG Preprocessing

Both grasping-related and ICMS-evoked EMG data were band-pass filtered, notch filtered, amplified, and digitized by hardware, as described elsewhere (Overduin et al., 2008), and then further band-pass filtered and full-wave rectified. Grasp-related EMG data were integrated within 9 ms (G1) or 11 ms (G2) bins, depending on the relative speed of the animal's movements. ICMS-evoked EMG data were instead integrated between 25 and 150 ms from the onset of each ICMS train. For grasp-related data, trials were time-aligned on the moment of object removal from the first well, truncated to windows of 100 samples spanning [–350:+550] ms (G1) or [–500:+600] ms (G2) around this moment, and averaged over the 40 trials in each of the 50 object conditions. Each channel was normalized to its maximum integrated EMG level observed over these averaged trials. The same normalization factors were applied to the ICMS-evoked data. These software preprocessing steps, as well as the subsequent analyses, were done in MATLAB (MathWorks).

Kinematic Analysis

Kinematic "convergence" was defined as a reduction in joint distance from a mean posture observed across trials. Using Figure 1B as an example, absolute displacements between the nine black dots (defining hand posture at 25 ms into ICMS, over nine stimulation trials) and their mean were calculated for each joint dimension (e.g., a1). This was then repeated for the nine lightest gray dots defining hand posture at 150 ms into ICMS by taking these points' absolute displacements from their mean. These two sets of numbers were compared using a one-sided t test to see whether the displacement had decreased significantly by 150 ms into ICMS. This comparison was repeated for all combinations of joints to find those stimulation sites with significant convergence in one or more joint dimensions ($p < 0.05$, Bonferroni corrected for the number of comparisons involving each joint). For illustration purposes, Figure 1B includes an ellipse defining the mean ± SD of all the intersection points between nine straight-line trajectories passing through each pair of black and lightest gray dots.

Synergy Extraction

For each subject, NNMF was used to identify a set of synchronous muscle synergies underlying either the grasp-related EMG data, $\boldsymbol{G}$, or the EMG patterns elicited by ICMS, $\boldsymbol{I}$. Each of the $O = 50$ object conditions in $\boldsymbol{G} = \boldsymbol{G}(e,s,o)$ was represented by $S = 100$ samples of integrated data in each of the E EMG channels, so the dimensionality of $\boldsymbol{G}$ was 15 × 100 × 50 (monkey G1) or 19 × 100 × 50 (G2). The ICMS-evoked data $\boldsymbol{I} = \boldsymbol{I}(e,t,l)$ included the E-channel EMG vectors evoked over the initial $T = 7$ trains delivered at each of the L ICMS locations (Figure 2), so the dimensionality of $\boldsymbol{I}$ was 15 × 7 × 33 (G1) or 19 × 7 × 13 (G2). The NNMF decompositions (Lee and Seung, 1999; Tresch et al., 1999) allowed EMG activity to be reconstructed as a combination of the corresponding $n = 1,\ldots,N_{grasp}$ or $1,\ldots,N_{icms}$ synergy vectors, each expressing a unique coactivation across $e = 1,\ldots,E$ EMG channels. Concatenated over synergies, these vectors could be compactly represented as $\boldsymbol{V}_{grasp}(e,n)$ or $\boldsymbol{V}_{icms}(e,n)$. In these EMG reconstructions, each synergy was weighted by nonnegative coefficients $\boldsymbol{W}_{grasp}(n,s,o)$ or $\boldsymbol{W}_{icms}(n,t,l)$ that could vary both within conditions (i.e., over time samples s or ICMS trains t) and across conditions (i.e., over object conditions o or locations l). In matrix form, these reconstructions could be expressed as:

$$\boldsymbol{G}(e,s,o) = \boldsymbol{V}_{grasp}(e,:) \cdot \boldsymbol{W}_{grasp}(:,s,o) \quad (1)$$

$$\boldsymbol{I}(e,t,l) = \boldsymbol{V}_{icms}(e,:) \cdot \boldsymbol{W}_{icms}(:,t,l) \quad (2)$$

where the colon operator indicates a vector of data in the matrix indexed by e, s, o, etc. For a given dimensionality N_{grasp} or N_{icms}, the algorithms iteratively updated synergies $\boldsymbol{V}_{grasp}$ and $\boldsymbol{V}_{icms}$, and associated weights $\boldsymbol{W}_{grasp}$ and $\boldsymbol{W}_{icms}$, until the total reconstruction error (R^2, the fraction of variance accounted for) grew by less than 0.001 over ten iterations. The synergies able to explain the most EMG variation over five repetitions of the algorithm were chosen for further analysis.

Synergy Comparison

To facilitate comparisons across animals and data sets, we set each of the dimensionalities N_{grasp} and N_{icms} to the number of synergies able to account for ≥95% of the variability in the corresponding data sets $\boldsymbol{G}$ (Figure 3B) and $\boldsymbol{I}$ (Figure 3C). In comparing synergies for each animal (Figure 3D), a greedy search procedure was used. First, dot products were computed for all $N_{grasp} \times N_{icms}$ possible pairs of grasp-related versus ICMS-derived synergies (e.g., 8 × 6 = 48 dot products, in the case of G2). Second, the best-matching grasp-related versus ICMS-derived pair was defined to be the one with the highest dot product. The second-best match was the one with the highest dot product among the remaining $(N_{grasp} - 1) \times (N_{icms} - 1)$ synergy pairs (7 × 5 = 35 for G2), and so on. This process continued until there were no more unpaired synergies left in one set ($min(8,6) = 6$ iterations for G2; Tresch et al., 1999). The significance of each matched pair was determined by Monte Carlo simulation. For each monkey, the greedy search procedure was run 10,000 times, each time after randomly shuffling muscle identity. Then the dot product of the best-matched pair of *actual* grasp-related and ICMS-derived synergies was compared with the distribution of dot products from the 10,000 best-matched pairs of *shuffled* synergies—or more precisely, with the 95th percentile of this distribution, as this defined a threshold for significant similarity at $p < 0.05$. The process was then repeated for the second-best pair of actual synergies versus the 10,000 second-best pairs of shuffled synergies, and so on. These procedures were also used to compare ICMS-derived synergies between G1 and G2, after first restricting the synergies to the 12 channels common to both animals (Figure 3D).

Cortical Analysis

Each animal's cortical topography of ICMS-derived muscle synergies (Figure 4) was tested for nonuniformity as follows. First, the degree to which a given synergy n was represented at a given ICMS location l was taken to be the mean coefficient $\boldsymbol{W}_{icms}(n,t,l)$ over $t = 1,\ldots,7$ ICMS trains delivered at the site, i.e., $\overline{\boldsymbol{W}_{icms}(n,:,l)}$. (The $\overline{\boldsymbol{W}_{icms}(n,:,l)}$ values are indicated in Figure 4 by the width of each circle.) For each ICMS location l, 10,000 vectors each of 33 (G1) or 13 (G2) values were randomly taken from a uniform distribution with the same mean and SD as the observed $\overline{\boldsymbol{W}_{icms}(n,:,l)}$. Second, the 95th percentile of the 10,000 maximum values from each vector was selected. Any observed $\overline{\boldsymbol{W}_{icms}(n,:,l)}$ values in excess of this threshold were deemed to reflect significant nonuniformity in the cortical representation of synergy n, peaking around cortical location(s) l ($p < 0.05$, Bonferroni-corrected for the number of synergies and the number of locations).

ACKNOWLEDGMENTS

This project was supported by NIH (NINDS) grant NS44393 to E.B. and a Dystonia Medical Research Foundation fellowship to S.A.O. We thank M. Cantor, C. Potak, J. Roh, S. Szczepanowski, and F. Zaheer for their assistance.

Accepted: October 10, 2012
Published: December 19, 2012

REFERENCES

Aoyagi, Y., Stein, R.B., Mushahwar, V.K., and Prochazka, A. (2004). The role of neuromuscular properties in determining the end-point of a movement. IEEE Trans. Neural Syst. Rehabil. Eng. *12*, 12–23.

Bizzi, E., Mussa-Ivaldi, F.A., and Giszter, S. (1991). Computations underlying the execution of movement: a biological perspective. Science *253*, 287–291.

Brochier, T., Spinks, R.L., Umiltá, M.A., and Lemon, R.N. (2004). Patterns of muscle activity underlying object-specific grasp by the macaque monkey. J. Neurophysiol. *92*, 1770–1782.

d'Avella, A., Saltiel, P., and Bizzi, E. (2003). Combinations of muscle synergies in the construction of a natural motor behavior. Nat. Neurosci. *6*, 300–308.

Drew, T., Kalaska, J., and Krouchev, N. (2008). Muscle synergies during locomotion in the cat: a model for motor cortex control. J. Physiol. *586*, 1239–1245.

Ethier, C., Brizzi, L., Darling, W.G., and Capaday, C. (2006). Linear summation of cat motor cortex outputs. J. Neurosci. *26*, 5574–5581.

Fetz, E.E., and Cheney, P.D. (1978). Muscle fields of primate corticomotoneuronal cells. J. Physiol. (Paris) *74*, 239–245.

Gentner, R., and Classen, J. (2006). Modular organization of finger movements by the human central nervous system. Neuron *52*, 731–742.

Giszter, S.F., Mussa-Ivaldi, F.A., and Bizzi, E. (1993). Convergent force fields organized in the frog's spinal cord. J. Neurosci. *13*, 467–491.

Graziano, M.S.A., and Aflalo, T.N. (2007). Mapping behavioral repertoire onto the cortex. Neuron *56*, 239–251.

Graziano, M.S.A., Taylor, C.S.R., and Moore, T. (2002). Complex movements evoked by microstimulation of precentral cortex. Neuron *34*, 841–851.

Graziano, M.S.A., Cooke, D.F., Taylor, C.S.R., and Moore, T. (2004a). Distribution of hand location in monkeys during spontaneous behavior. Exp. Brain Res. *155*, 30–36.

Graziano, M.S.A., Patel, K.T., and Taylor, C.S.R. (2004b). Mapping from motor cortex to biceps and triceps altered by elbow angle. J. Neurophysiol. *92*, 395–407.

Graziano, M.S.A., Aflalo, T.N., and Cooke, D.F. (2005). Arm movements evoked by electrical stimulation in the motor cortex of monkeys. J. Neurophysiol. *94*, 4209–4223.

Griffin, D.M., Hudson, H.M., Belhaj-Saïf, A., and Cheney, P.D. (2011). Hijacking cortical motor output with repetitive microstimulation. J. Neurosci. *31*, 13088–13096.

Haiss, F., and Schwarz, C. (2005). Spatial segregation of different modes of movement control in the whisker representation of rat primary motor cortex. J. Neurosci. *25*, 1579–1587.

Hart, C.B., and Giszter, S.F. (2010). A neural basis for motor primitives in the spinal cord. J. Neurosci. *30*, 1322–1336.

Kargo, W.J., and Nitz, D.A. (2003). Early skill learning is expressed through selection and tuning of cortically represented muscle synergies. J. Neurosci. *23*, 11255–11269.

Lee, D.D., and Seung, H.S. (1999). Learning the parts of objects by non-negative matrix factorization. Nature *401*, 788–791.

Lemon, R.N. (1993). The G. L. Brown Prize Lecture. Cortical control of the primate hand. Exp. Physiol. *78*, 263–301.

Loeb, E.P., Giszter, S.F., Borghesani, P., and Bizzi, E. (1993). Effects of dorsal root cut on the forces evoked by spinal microstimulation in the spinalized frog. Somatosens. Mot. Res. *10*, 81–95.

Mason, C.R., Theverapperuma, L.S., Hendrix, C.M., and Ebner, T.J. (2004). Monkey hand postural synergies during reach-to-grasp in the absence of vision of the hand and object. J. Neurophysiol. *91*, 2826–2837.

Mussa-Ivaldi, F.A., Giszter, S.F., and Bizzi, E. (1990). Motor-space coding in the central nervous system. Cold Spring Harb. Symp. Quant. Biol. *55*, 827–835.

Nelson, R.J., McCandlish, C.A., and Douglas, V.D. (1990). Reaction times for hand movements made in response to visual versus vibratory cues. Somatosens. Mot. Res. *7*, 337–352.

Overduin, S.A., d'Avella, A., Roh, J., and Bizzi, E. (2008). Modulation of muscle synergy recruitment in primate grasping. J. Neurosci. *28*, 880–892.

Overduin, S.A., Zaheer, F., Bizzi, E., and d'Avella, A. (2010). An instrumented glove for small primates. J. Neurosci. Methods *187*, 100–104.

Ramanathan, D., Conner, J.M., and Tuszynski, M.H. (2006). A form of motor cortical plasticity that correlates with recovery of function after brain injury. Proc. Natl. Acad. Sci. USA *103*, 11370–11375.

Rathelot, J.A., and Strick, P.L. (2009). Subdivisions of primary motor cortex based on cortico-motoneuronal cells. Proc. Natl. Acad. Sci. USA *106*, 918–923.

Roh, J., Cheung, V.C., and Bizzi, E. (2011). Modules in the brain stem and spinal cord underlying motor behaviors. J. Neurophysiol. *106*, 1363–1378.

Saltiel, P., Wyler-Duda, K., D'Avella, A., Tresch, M.C., and Bizzi, E. (2001). Muscle synergies encoded within the spinal cord: evidence from focal intraspinal NMDA iontophoresis in the frog. J. Neurophysiol. *85*, 605–619.

Santello, M., Flanders, M., and Soechting, J.F. (1998). Postural hand synergies for tool use. J. Neurosci. *18*, 10105–10115.

Schieber, M.H. (2001). Constraints on somatotopic organization in the primary motor cortex. J. Neurophysiol. *86*, 2125–2143.

Stepniewska, I., Fang, P.C., and Kaas, J.H. (2005). Microstimulation reveals specialized subregions for different complex movements in posterior parietal cortex of prosimian galagos. Proc. Natl. Acad. Sci. USA *102*, 4878–4883.

Strick, P.L. (2002). Stimulating research on motor cortex. Nat. Neurosci. *5*, 714–715.

Takei, T., and Seki, K. (2010). Spinal interneurons facilitate coactivation of hand muscles during a precision grip task in monkeys. J. Neurosci. *30*, 17041–17050.

Torres-Oviedo, G., and Ting, L.H. (2007). Muscle synergies characterizing human postural responses. J. Neurophysiol. *98*, 2144–2156.

Tresch, M.C., and Bizzi, E. (1999). Responses to spinal microstimulation in the chronically spinalized rat and their relationship to spinal systems activated by low threshold cutaneous stimulation. Exp. Brain Res. *129*, 401–416.

Tresch, M.C., Saltiel, P., and Bizzi, E. (1999). The construction of movement by the spinal cord. Nat. Neurosci. *2*, 162–167.

Zimmermann, J.B., Seki, K., and Jackson, A. (2011). Reanimating the arm and hand with intraspinal microstimulation. J. Neural Eng. *8*, 054001.